Dual Functionalized Bacteriophage Qβ as a Photocaged Drug Carrier

*Zhuo Chen, Na Li, Luxi Chen, Jiyong Lee, and Jeremiah J. Gassensmith**

Proteinatious nanoparticles are emerging as promising materials in biomedical research owing to their many unique properties and our interest focuses on integrating environmental responsivity into these systems. In this work, the use of a virus-like particle (VLP) derived from bacteriophage Qβ as a photocaged drug delivery system is investigated. Ideally, a photocaged nanoparticle platform should be harmless and inert without activation by light yet, upon photoirradiation, should cause cell death. Approximately 530 photocleavable doxorubicin complexes are installed initially onto the surface of Qβ by CuAAC reaction for photocaging therapy; however, aggregation and precipitation are found to cause cell death at higher concentrations. In order to improve solution stability, thiol-dibromomaleimide chemistry has been developed to orthogonally modify the VLP. This chemistry provides a robust method of incorporating additional functionality at the disulfides on Qβ, which was used to increase the stability and solubility of the drug-loaded VLPs. As a result, the dual functionalied VLPs with polyethylene glycol and photocaged doxorubicin show not only negligible cytotoxicity before photoactivation but also highly controllable photorelease and cell killing power.

1. Introduction

Nanotechnology based on virus-like particles (VLPs) is an emerging interdisciplinary field connecting chemistry, biology, and material science around noninfectious viral analogues. The growing interest in VLPs is owed to their nanometer size, monodispersity, polyvalency, biocompatibility, and the ability to functionalize their surfaces by both chemical and genetic modification with atomistic precision. These features have made VLPs a promising platform for biomedical research and they are clearly emerging[1–3] as enticing tools in the biomedical arena in both therapeutic[4] and diagnostic[5–7] roles. As the recombinantly expressed and noninfectious structural analogue of a virus, VLPs are still imbued with their native viral resilience against environmental attack,[8–13] yet as nanometer-sized macromolecular ensembles, their size, shape, and chemical addressability have allowed them to serve as multivalent scaffolds[14–17] for the attachment of densely packed MRI contrast agents,[18–20] fluorescent dyes,[21–24] and therapeutics.[25–27] Appropriately functionalized, VLPs show passive tumor accumulation[28] by the enhanced permeability and retention effect[29,30] yet still have clinically useful and tunable[31] circulation half-lives—a quality notoriously difficult to imbue into metallic or inorganic nanoparticles.

A key area of our interest is integrating these protein-based nanoparticles with chemically switchable[27,32–34] systems—that is, using environmental stimuli to control the release of material from their surfaces—a developing area that has seen the emergence of protein[35] and peptide[36,37]-based smart systems. While early studies have

Z. Chen, Dr. N. Li, Dr. L. Chen, Prof. J. Lee, Prof. J. J. Gassensmith
Department of Chemistry and Biochemistry
The University of Texas at Dallas 800 West Campbell Road
Richardson, TX 75080-3021, USA
E-mail: gassensmith@utdallas.edu

DOI: 10.1002/smll.201601053

focused on using controlled degradation of polymers graphed to or inside VLPs to afford drug release, we chose to focus instead on integrating small molecule photocaged[38–40] therapeutics—that is, therapeutics that are biologically inert unless photolytically cleaved from the surface of the VLP. The benefit of this approach is that it would allow clinicians to activate a drug site—specifically using either laser or fiber optic phototherapy,[41] thus avoiding off-target dosing, which is associated with many of the negative side effects of current chemotherapies. The use of photocaging biologically active small molecules is emerging as a promising technique for site-specific delivery, as it allows significant tunability by judicious choice of photolinker and therapeutic. By combining the photocaging strategy with the extensible architecture of VLP nanoparticles, we aim to produce a platform that delivers the anticancer drug doxorubicin (Dox) into a tumor environment; yet, as an inactivated complex, Dox is unable to access the cellular DNA until the small molecules are cleaved from the nanoparticle.

For this work, we utilized an icosahedral VLP derived from bacteriophage Qβ, which self-assembles recombinantly within *E. coli*. The 28 nm diameter capsid is composed of 180 identical coat-protein subunits. Qβ is relatively stable to high temperatures (<80 °C), extremes in pH, and organic cosolvent. Partial functionalization of the 720 solvent-exposed amino groups on the surface is known[27] and proceeds in good yields. Additionally, Qβ possesses two cysteine residues per coat protein, which reside at the three- and five-fold axis of symmetry in the quaternary structure.[9,17] These cysteine residues link the individual monomers into either hexameric or pentameric subunits, which help increase the overall thermal stability of the capsid. (**Figure 1**)

Here, we discuss our approach toward the rational design of a VLP-based photocaged therapeutic and show that in its inactive form, it lacks cytotoxicity even at high concentrations, yet when activated it shows efficacy similar to free Dox. Our initial efforts to simply append doxorubicin to the surface exposed amines of the VLP resulted in aggregation-induced precipitation of the Dox-VLP complex. To overcome this, we exploited a method to dual functionalize the VLP surface at the solvent exposed disulfide residues to evenly distribute polyethylene glycol (PEG) units to aid in solubilizing the conjugate.[42] We employed a cysteine rebridging strategy that affords bespoke functionality yet retains the covalent character of the disulfide bridge. This strategy worked and has potential to become particularly

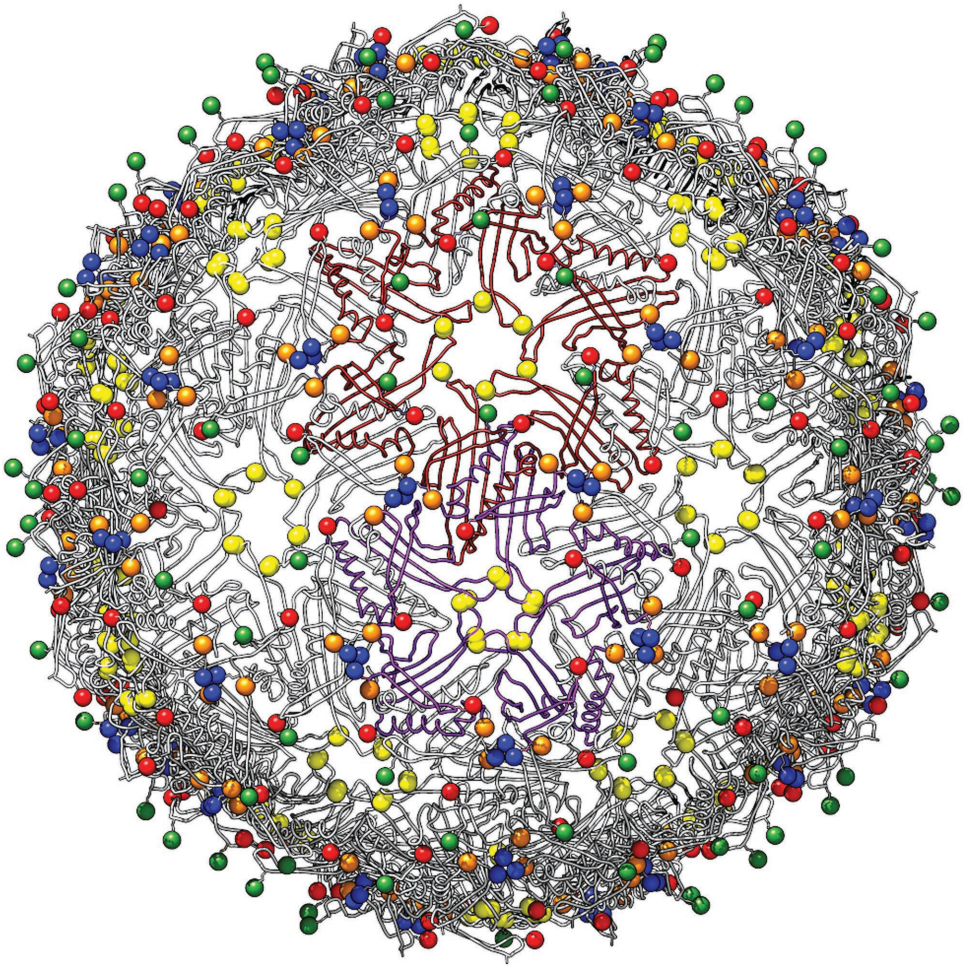

Figure 1. VLP Qβ is composed of 180 identical coat proteins, each with four solvent exposed primary amines, *N*-termini = orange, K2 = blue, K13 = red, K16 = green. These monomers are connected by disulfides (yellow) to form several interlinked subunits of either five (the pentameric subunit colored purple) or six (the hexameric subunit colored brown) coat proteins.

DOI: 10.1002/smll.201601053

enabling toward immune passivation,[31,43] attachment of targeting ligands,[44] or functionalization with contrast agents[45] to create theranostic nanoparticle[30] conjugates. We were then able to create dual-functionalized VLPs which showed negligible toxicity to breast cancer cells in the absence of activation yet was highly cytotoxic upon activation.

2. Results and Discussion

Our initial approach toward the synthesis of photocaged Dox-Qβ is outlined in **Scheme 1**. We selected the nitroveratryl compound **2** as the photocleavable linker between the Dox and the azide functionalized surface of Qβ owing to its (1) ease of preparation, (2) it is cleaved under long-wavelength UV-A light, which is clinically used in photochemotherapy for cutaneous T-cell lymphoma as well as in a variety of skin diseases,[46,47] and (3) the fact it reversibly quenches the ordinarily fluorescent Doxorubicin. This reversible quenching provides a diagnostic indictor to determine the efficacy of photorelease; as soon as the Dox is photolytically cleaved from Qβ—and the nitroveratryl linker—it becomes fluorescent again.

Following functionalization of the exposed primary amines with 7-azidoheptanoic acid *N*-hydroxysuccinimide (compound **1** from Scheme 1), linker **3** was ligated to Qβ-N_3 under copper-catalyzed azide-alkyne cycloaddition (CuAAC) conditions. Denaturing gel electrophoresis (SDS-PAGE) analysis under reducing conditions was used to confirm covalent conjugation to the 14.2 kDa monomeric coat protein. As seen in **Figure 2**, Qβ_r-Dox, UV(–), conjugation is evident from new bands at higher positions, indicative of attachment of one to three copies of Linker **3** with the majority being triply functionalized. This result was further reinforced via quantification carried out by solution state UV–vis absorption collected at 490 nm (λ_{max} of Dox), which was used to determine that an average of 520 ± 65 Dox molecules were attached to a single Qβ particle. This roughly corresponds to 2.8 linkers for each of the 180 coat proteins on Qβ.

We then investigated the solution state kinetics of photocleavage, which (Figure S2, Supporting Information) revealed that photolytic activation of the caged species has an average $T_{1/2}$ of 4.2 min, corresponding to a 90% release of Dox within 15 min of exposure to a 4W UV-lamp. The photolytic cleavage was further assayed using reducing SDS-PAGE. Compared to control Qβ-Dox, which was not exposed to UV (Figure 2, Qβ_r-Dox, UV(–)), the photolytically cleaved Qβ-Dox (Figure 2, Qβ_r-Dox,UV(+)) returns to roughly the same position as unfunctionalized monomer coat protein and the released fluorescent Dox molecules run to the front of the gel. Taken together, it is clear that we can photolytically release Dox under these relatively mild conditions allowing us to move to Qβ-Dox in vitro.

2.1. Cytotoxicity Assay of Qβ-Dox

We next investigated whether the attachment of Dox to Qβ via the nitroveratryl moiety would enable photocontrolled drug delivery to cells. Breast cancer cell line MCF-7 was incubated with varying concentrations of Qβ-Dox or

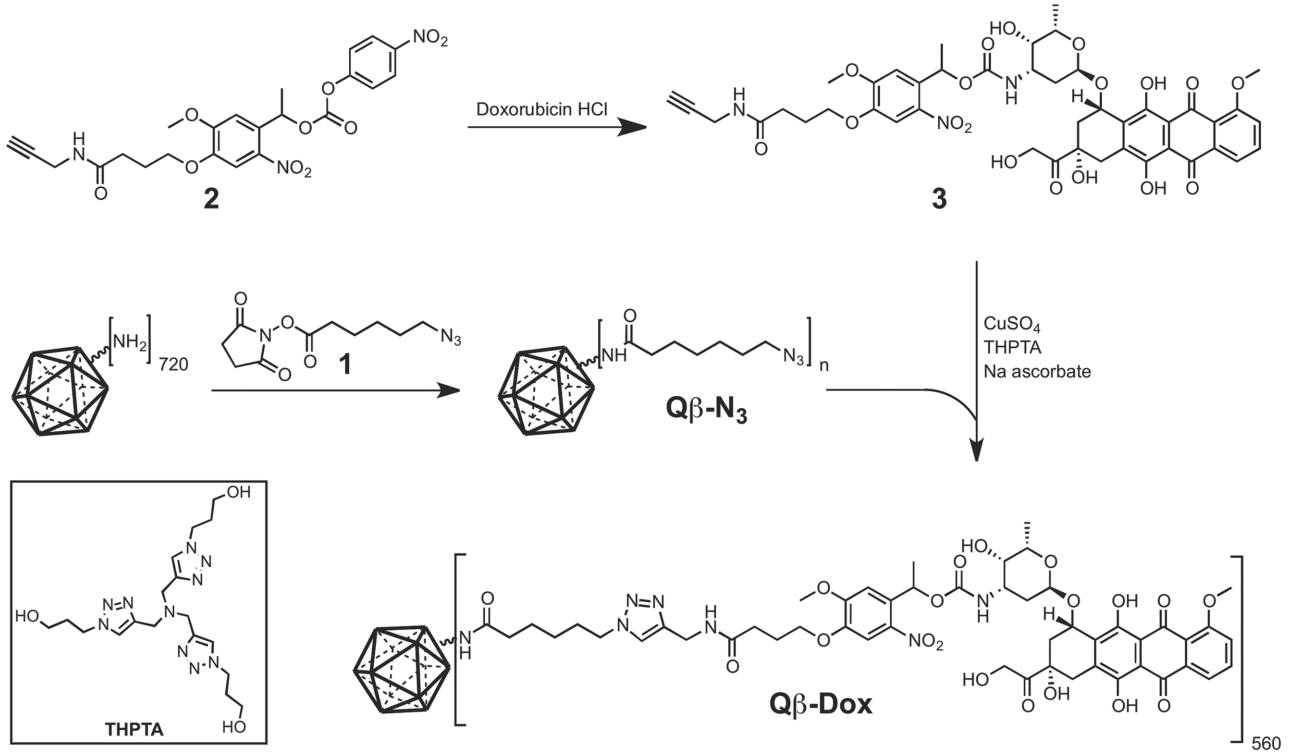

Scheme 1. Synthesis of Qβ-Dox conjugates. Qβ was labeled by azide moiety by reaction between primary amines of Qβ and 7-azidoheptanoic acid *N*-hydroxysuccinimide. Compound **3** was synthesized by a reaction between doxorubicin and photocleavable linker **2** with an alkynyl moiety. Then doxorubicin was ligated to Qβ by CuAAC reaction between the azide group on Qβ-N_3 and the alkynyl group of **3**.

DOI: 10.1002/smll.201601053

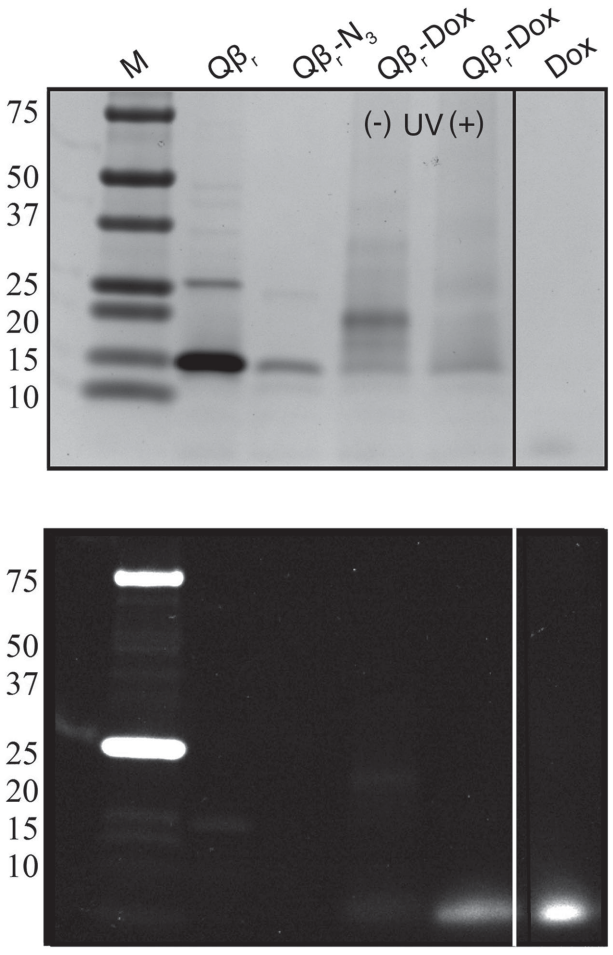

Figure 2. Reducing SDS-PAGE showing Qβ, Qβ conjugates, and photorelease assay (UV lamp: 4 W, 365 nm, 15 min). Under reducing conditions, the pentameric and hexameric subunits are reduced to the monomeric coat protein (Qβ_r). Image of Coomassie blue stain (top) and unstained gel fluorescence image (bottom). Fluorescence is from Dox or Marker. After photorelease, the main protein band is closer to Qβ-N_3, while the fluorescent released Dox has a same position with free doxorubicin.

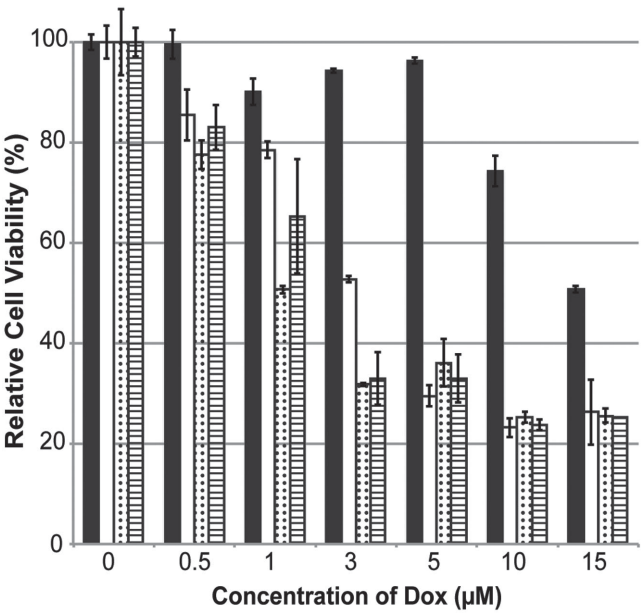

Figure 3. MTT cell viability assay following exposure to select reagents at different concentrations. Lighter shade indicates UV light exposure. Displayed—in order and by color—Black: Qβ-Dox kept in the dark; White: Qβ-Dox after 15 min of UV exposure; White with dots: Doxorubicin kept in the dark; White with bars: Doxorubicin after 15 min of UV exposure.

appropriate controls which were either left in the dark or were subjected to 15 min of UV exposure. Cell viability was subsequently measured by MTT assay (**Figure 3**). Following UV exposure, the Qβ-Dox exhibited concentration dependent cytotoxicity comparable to free Dox at higher concentrations. While the activated complexes demonstrated the anticipated behavior, unactivated Qβ-Dox showed some degree of toxicity in the dark across all concentrations. Our initial concern was that the Qβ-Dox complex was being degraded by lysosomal activity following cellular uptake, causing Dox release in the dark. While confocal microscopy clearly shows cellular uptake of these complexes (Figure S22–S25, Supporting Information), we were able to partly rule out digestive release of Dox by showing a lack of significant DNA damage[48] in cell cultures incubated in the dark by PARP analysis (Figure S7, Supporting Information), indicating the cells were neither being killed by Dox nor undergoing normal apoptosis. We thus concluded that the cytotoxicity is related to the Qβ-Dox conjugate's tendency to aggregate and precipitate from solution—likely a result of attaching more than 500 hydrophobic Dox molecules to the surface. As seen in the optical photographs in **Figure 4** and Figure S3 (Supporting Information), this precipitation of Qβ-Dox occurs in both solution and in cell culture. This precipitation behavior necessitated a reevaluation of our approach. To solve this problem, we rationalized that increasing the solution stability of the Qβ-Dox colloidal suspension by attaching PEG residues to the capsid may promote solution stability and prevent this behavior. Based on previously published[30] analyses of PEG-coated VLP surfaces, which show that short chain PEGs form mushroom-shaped domains that rise above the surface of VLPs, we reasoned it would be unlikely that the PEG chains would impede the photolytic activation and release of the Dox from the surface bound ligands. Beyond the practical issues we were facing with precipitation, functionalization of PEG would allow us to create stealth particles[31] that can evade immune recognition. We thus needed a means of distributing the PEGs across the surface of Qβ. One option would be to simply sacrifice a percentage of the surface bound amines for PEGylation by first functionalizing the exposed lysines with substoichiometric amounts of Dox and then attaching PEGs to the remaining lysines. While possible, this strategy is undesirable, as it would sacrifice valuable surface exposed lysines to make way for PEGgylation thus reducing Dox loading. We thus sought a means of attaching surface ligands to Qβ using the solvent exposed disulfides, yet in a way that did not sacrifice the capsid's stability.

2.2. Functionalization of Disulfides on Qβ

As previously discussed, each of the 180 identical coat proteins possesses two cysteine residues—Cys 74 and Cys 80—which

DOI: 10.1002/smll.201601053

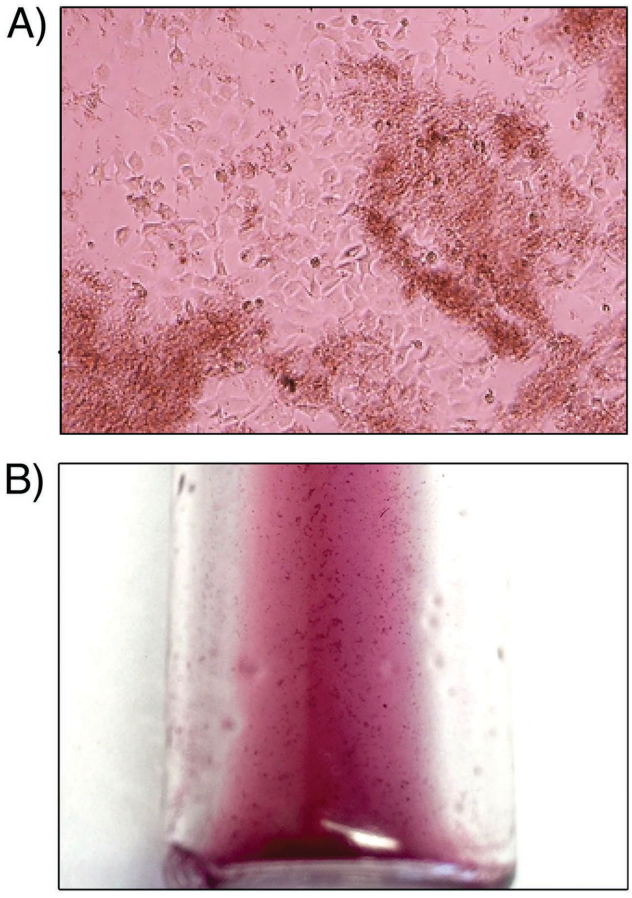

Figure 4. Optical photographs showing precipitation of 30×10^{-6} M Qβ-Dox in (A) the MCF-7 cell culture and (B) an aqueous solution. Small punctate particles are precipitates.

form a disulfide bridge to a neighboring coat protein. Cys 74 of one protein monomer connects to Cys 80 of an adjacent monomer and daisy chains to form either a cyclic hexamer—colored brown in Figure 1—or a pentamer—colored purple in the same Figure. We sought to use these solvent exposed disulfides as sites for bioconjugation but we did not want to lose all of the thermal stability afforded by the disulfide bridges,[11] which would happen if we simply reduced them to the free thiols and then functionalized the discrete sulfhydryl groups. Instead, we opted for a strategy using a reagent recently described[49] by Baker and Caddick that would allow us to "rebridge" a reduced disulfide using a dibromo-functionalized maleimide (**Figure 5**). While this reagent has proven effective in cross-linking disulfides on the same peptide or in the dimerization of two antibodies,[50] the ability to effectively "restich" five or six coat protein monomers back into their respective cyclic oligomers outwardly appears entropically uphill.

The disulfides can be quantitatively reduced using five eq of tris(2-carboxyethyl)phosphine (TCEP) per disulfide at ambient temperature in 30 min. Reduction was monitored by nonreducing SDS-PAGE (**Figure 6**a). A small amount of dimer persists because of strong hydrophobic interaction between proteins.[17] Interestingly, samples of Qβ capsid that are spectroscopically pure by fast protein liquid chromatography (FPLC) analysis show lower order oligomeric protein subunits on nonreducing SDS-PAGE, suggesting that not all the disulfides on Qβ are oxidized following expression in *E. coli*. This does not present a problem for our chemistry, since the disulfides must be reduced prior to functionalization anyway.

Because analysis of PEGylation—an uncharged, largely inert, and colorless polymer—tends to be indirect, we wanted to ascertain the efficacy of this disulfide functionalization reaction using a simple small molecule conjugate. To that end, a dibromomaleimide-fluorescein derivative (DB-MF) was synthesized and used to functionalize Qβ nanoparticles—Qβ(MF)—which were analyzed by UV–vis spectrum (Figure S1, Supporting Information), nonreducing SDS-PAGE and visualized by fluorescence (Figure 6) and Coomassie blue staining. The fluorescence signal observed in the SDS-PAGE primarily belonged to the hexamer and pentamer bands with faint signal from the lower-order subunits. Quantification of the reaction was done using solution-state UV–vis spectroscopy, which gave an overall yield of 98%—nearly 180 copies of fluorescein per particle. These data strongly indicate that DB-MF is bound covalently to the subunits and largely reforms the hexamer and pentamers following reduction using TCEP. We were further able to confirm that the rebridged substrates were stable in the presence of moderate amounts of TCEP, though the reaction readily undergoes an anti-Michale addition in the presences of dithiothreitol (DTT), in accord with Baker and Caddick's early findings.[49] The integrity of these fluorescent

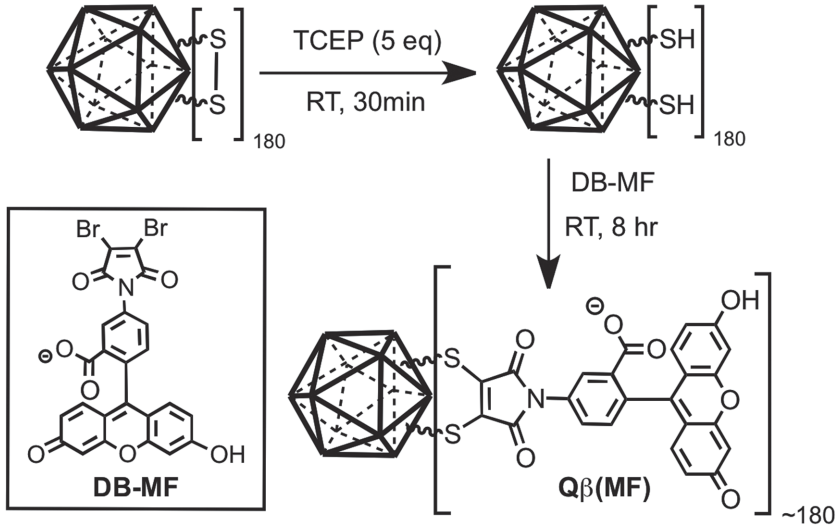

Figure 5. Rebridging disulfides on Qβ with fluorescein-functionalized dibromomaleimide (DB-MF). The disulfides on Qβ are reduced using five eq. of TCEP at room temperature (RT) within 30 min. The free sulfhydryl functions are then rebridged over the course of 12 h following addition of DB-MF in buffer at RT.

DOI: 10.1002/smll.201601053

www.MaterialsViews.com

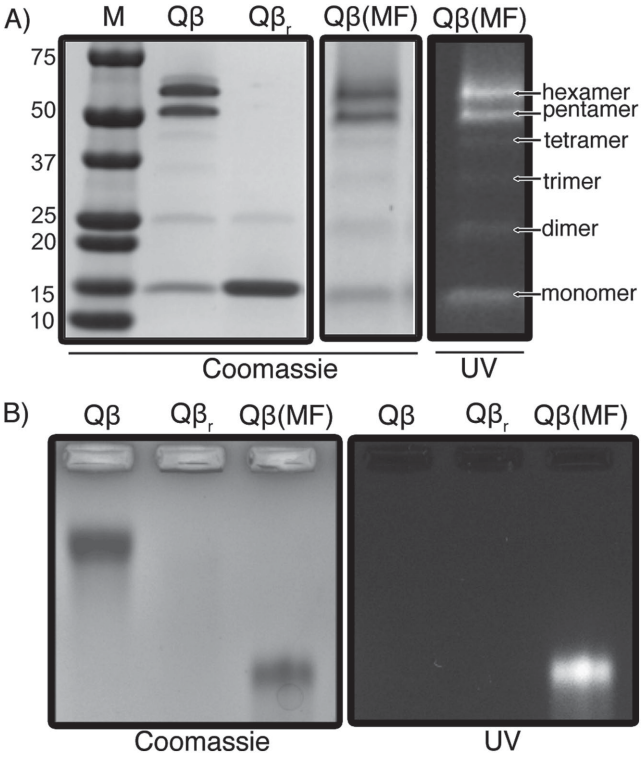

Figure 6. Characterization of Qβ (MF) conjugate. A) Nonreducing SDS-PAGE shows intact protein subunits. Though the capsid is pure by FPLC analysis, small amounts of lower order oligomers exist. M: protein marker. B) Native agarose shows electrophoretic mobility of the intact capsid and shown are the (left) Coomassie stained and (right) UV image of the same gel. The greater mobility of the fluorescently functionalized Qβ (MF) conjugate arises from its increased negative charge.

rebridged nanoparticles was confirmed by native agarose gel electrophoresis (Figure 6b). At the running buffer pH (9.0), Qβ(MF) traveled faster toward the positive electrode, since it carries more negative charge than the native Qβ particle. The fluorescent conjugate nanoparticle could be visualized well under UV illumination.

Finally, the apparent melting temperature of the conjugate nanoparticle was evaluated using far-UV circular dichroism (CD) spectroscopy following an established protocol for Qβ.[51] The thermal stability (Figure S15, Supporting Information) of the secondary structure in the Qβ(MF) conjugate was compared to the unmodified (1) oxidized and (2) reduced Qβ and we found these structures to denature at 87.0 ± 0.24 and 61.0 ± 1.03 °C, respectively, inline with previous reports.[9,51] The Qβ(MF) conjugate was then tested and a T_m of 73.7 ± 0.15 °C was calculated—midway to the native structure (Figure S11 and S12, Supporting Information). These results gave us confidence that the disulfides that line the pores of the Qβ could be used to further functionalize the surface of the nanoparticle in potentially high yields without significantly compromising the integrity of the VLP.

2.3. Synthesis and Cytotoxicity Assay of Qβ (MPEG)-Dox

Having worked out a general procedure to functionalize the disulfides of Qβ in good yield, we synthesized PEG-1000 and 2000 functionalized dibromomaleimides (DB-MPEG 1K and DB-MPEG 2K) and conjugated them to Qβ to form either Qβ(1K) or Qβ(2K) in accordance to **Scheme 2**. SDS-PAGE results shown in **Figure 7** and **8** make it clear that the pentamer and hexamer bands of Qβ exhibit a slight position change similar to those observed[30] in other systems, indicating covalent attachment with DB-MPEG 1K or DB-MPEG 2K. Further, we know the reemergence of the hexamer and pentamer bands does not occur because of simple reoxidation of the disulfides, as TCEP cannot rereduce these PEGylated structures to the monomer. Indeed, very high concentrations of DTT, which readily reduces disulfides, was only partially successful in removing the maleimide via an anti-Michale addition to the maleimide functionalized capsid (Figure 8). Analysis of thermal stability of the PEG

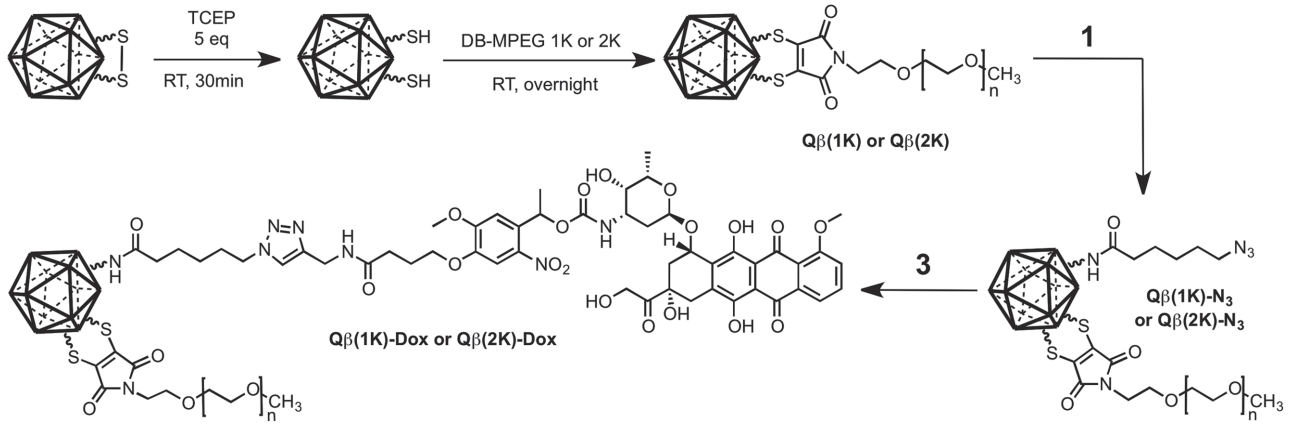

Scheme 2. Synthesis of Qβ(1K)-Dox or Qβ(2K)-Dox: The disulfides on Qβ are reduced using five eq of TCEP at RT in 30 min. The free sulfhydryl functions are then rebridged following addition of dibromomaleimide-functionalized PEG compounds (DB-MPEG 1K or DB-MPEG 2K). The doxorubicin was ligated to Qβ(1K) or Qβ(2K) using the same procedure as that for Qβ-Dox. Qβ(1K) or Qβ(2K) were reacted with compound **1** (7-azidoheptanoic acid *N*-hydroxysuccinimide) to affix azide groups to the surface of the capsid followed by reaction with **3** (doxorubicin-nitroveratryl derivative) via CuAAC reaction.

DOI: 10.1002/smll.201601053

small NANO MICRO

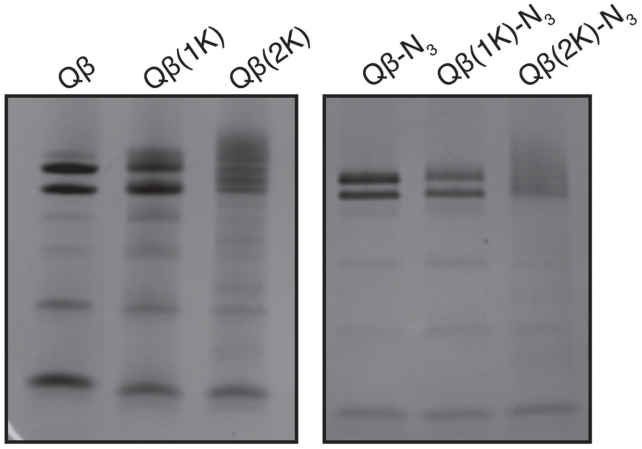

Figure 7. Nonreducing SDS-PAGE of Q*β* PEG conjugates and dual-functionalized Q*β* PEG-azide conjugates.

functionalized nanoparticles by CD spectroscopy revealed no apparent degredation of secondary structure even beyond 100 °C for the Q*β*(1K) formulation, while the thermal stability was approximately the same as the unfunctionalized

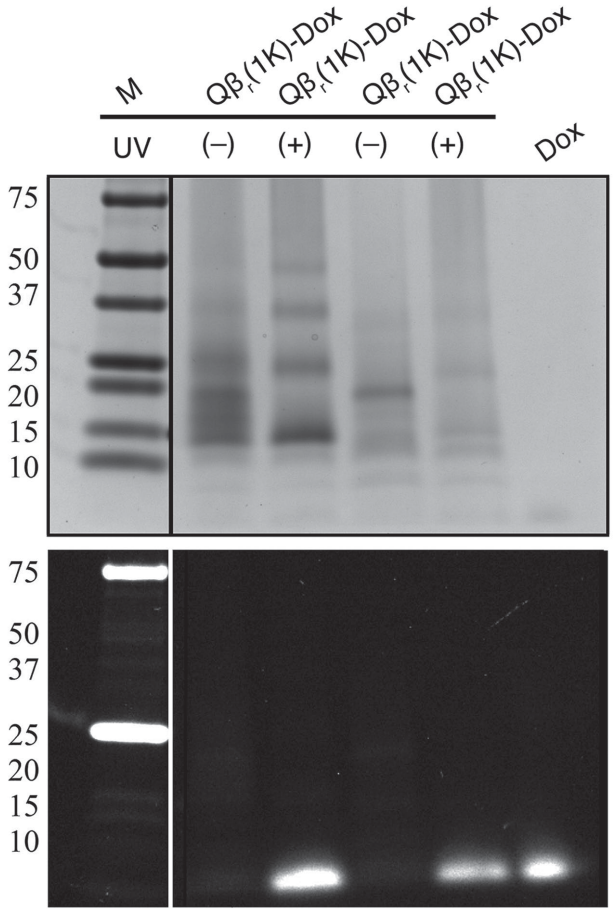

Figure 8. SDS-PAGE (w/DTT) of Q*β* (MPEG-Dox) conjugates showing both control and photolytically cleaved products (UV lamp: 4 W, 365 nm, 15 min). Image of Coomassie blue stain (top) and unstained fluorescent gel (bottom). DTT performs an anti-Michael addition to the maleimide, breaking the oligomers. Even at high concentrations of DTT, this reaction appears inefficient with Q*β* (1K)-Dox.

VLP for the Q*β*(2K) conjugate (Figure S13–S17, Supporting Information). This result is quite incredible, though similar thermally protective affects attributed to PEG have been previously reported for PEG-functionalized tobacco mosaic virus.[52] SDS-PAGE band intensities were measured by densitometry showing that DB-MPEG 1K attaches to the capsid in ≈90% yield. In other words, about 162 1K PEG chains attach to the capsid in total. Reactions using DB-MPEG 2K were difficult to quantify as the hexamer and pentamer bands streaked together on the gel, rendering densitometry analysis unreliable.[53] In any regard, it is obvious from band shifts that covalent attachment of MPEG 2K occurred, likely with an attenuated yield.

Dox was then attached to the PEGylated VLP Q*β*(1K) or Q*β*(2K) using the original procedure and characterized by reducing SDS-PAGE (Figure 8). When the reaction is performed in this order, the yield for Dox conjugation is still about 500 Dox molecules per VLP (Q*β*(1K)-Dox: 499 ± 52 Dox/Q*β*, Q*β*(2K)-Dox: 515 ± 64 Dox/Q*β*), a result that supports earlier claims of a mushroom-shaped configuration of PEG leaving the surface functions still wide open for additional chemistry. Interestingly, when we reversed the order of conjugation and attempted to attach DB-MPEG 1K or 2K to Q*β* already functionalized by Dox (Q*β*-Dox) we observed no attachment of PEG at all. We speculate this may be attributed to several factors—the way the Q*β*-Dox sits on the surface may block the disulfides or the observed precipitation likely affects reactivity, for instance.

Though transmission electron microscopy (TEM) micrographs show that both Q*β*(1K)-Dox and Q*β*(2K)-Dox continue to aggregate (Figure S8–S10, Supporting Information) when drop cast and dried onto a grid, they are more solution stable than Q*β*-Dox as shown by Zeta potential (Figure S4, Supporting Information) and dynamic light scattering (DLS) measurements (Figure S18–S20, Supporting Information).[54,55] The difference in aggregation behavior was further illustrated during confocal microscopy (Figure S22–S25, Supporting Information), which show significant fluorescent aggregates in the Q*β*-Dox experiments and yet little to no aggregates in the Q*β*(MPEG)-Dox studies. Experiments looking at the relative critical coagulation concentrations are ongoing. Cytotoxicity was again evaluated on MCF-7 cells using our Q*β*(MPEG)-Dox (**Figure 9** and Figure S5 and S6, Supporting Information). While this new formulation shows the same cell-killing power upon light activation, these samples showed much less cytotoxicity in the dark compared to Q*β*-Dox and had a similar cytotoxicity to controls without any Dox. This trend of improved cell viability in the dark became more obvious at higher concentrations. While the unPEGylated Q*β*-Dox VLP has an IC_{50} of 15×10^{-6} M, the PEGylated formulation did not show appreciable cytotoxicity over the range of our experiments. As a result, the high stability of Q*β*(MPEG)-Dox conjugates in the dark confirms this system is photocaged and can be highly controlled by photoirradiation for drug release. On the other hand, in the presence of PEG, it still maintains the ability to kill significant amount of cells following photolytic uncaging of the Dox.

DOI: 10.1002/smll.201601053

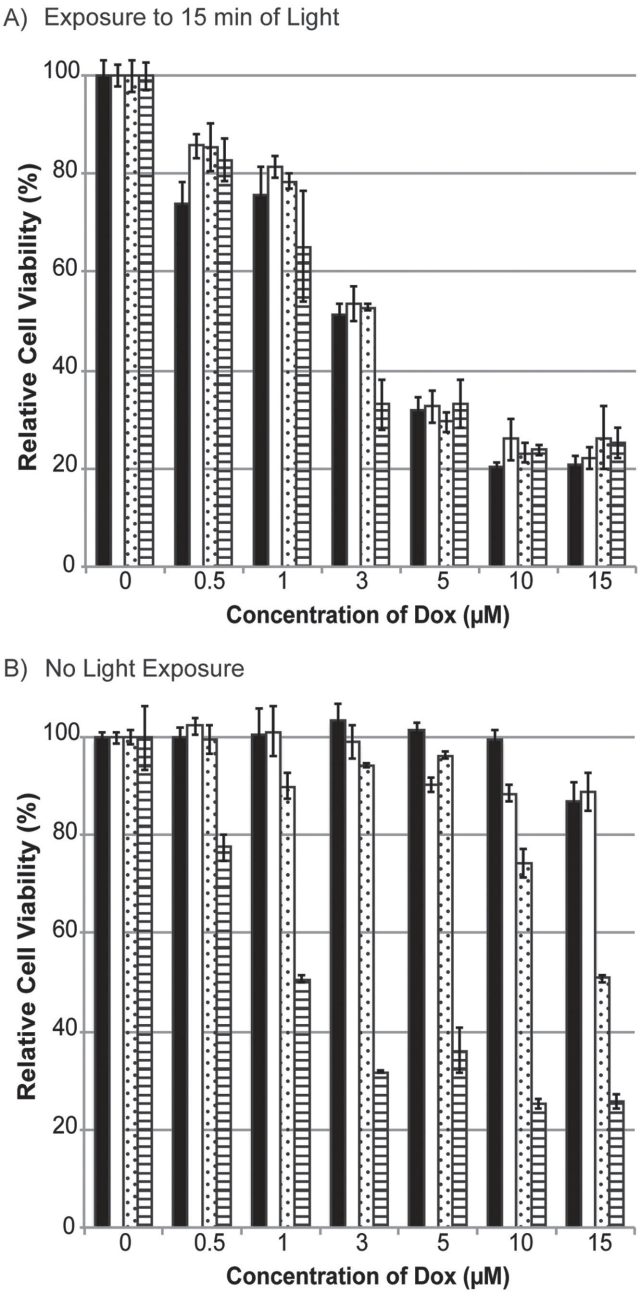

Figure 9. MTT Assay showing the relative cytotoxicities of the synthesized Qβ-Dox conjugates compared to free doxorubicin at different concentrations either as (A) activated or (B) photocaged complexes. Displayed—in order and by color—Black: Qβ(1K)-Dox; White: Qβ(2K)-Dox; White with dots: Qβ-Dox; White with bars: Free doxorubicin. The depicted graphs show the (A) cytotoxicity of activate conjugates and free Dox following exposure to 15 min of UV irradiation and (B) the relative cytotoxicity of the conjugates and free Dox if left in the dark.

3. Conclusion

Photocaging therapeutics to VLPs offers an extensible platform for high-drug loading and triggered release. Our initial efforts to attach the photocaged doxorubicin, a large and hydrophobic anticancer drug, to the surface of Qβ VLP lead to disappointing aggregation and precipitation at modest concentrations. We then developed methodology to modify the surface exposed disulfide residues of the VLP without compromising the thermal stability of the quaternary structure. Through the dual modification of the Qβ VLP scaffold, we were able to create a photocontrolled drug delivery system, which shows negligible cytotoxicity when the anticancer drugs are photocaged yet becomes quite cytotoxic following activation by light. This proof-of-principle design demonstrates the potential of not only the photocaging methodology but also the synthetic power of the disulfide rebridging reactions on these VLPs.

Supporting Information

Supporting Information is available from the Wiley Online Library or from the author.

Acknowledgements

Z.C. and N.L. contributed equally to this work. The authors thank M. G. Finn and Jenny Cheng for the plasmids used to express the VLPs and their helpful insight. They also thank Dr. Theodore Price and Galo Mejia for confocal imaging.

[1] N. F. Steinmetz, T. Lin, G. P. Lomonossoff, J. E. Johnson, in *Viruses and Nanotechnology*, Vol. *327* (Eds: M. Manchester, N. Steinmetz), Springer, Berlin **2009**, pp. 23–58.
[2] P. Singh, M. J. Gonzalez, M. Manchester, *Drug Dev. Res.* **2006**, *67*, 23.
[3] G. Destito, A. Schneemann, M. Manchester, in *Viruses and Nanotechnology*, Vol. *327* (Eds: M. Manchester, N. Steinmetz), Springer, Berlin **2009**, pp. 95–122.
[4] Y. Ma, R. J. M. Nolte, J. J. L. M. Cornelissen, *Adv. Drug Delivery Rev.* **2012**, *64*, 811.
[5] N. F. Steinmetz, *Nanomed.: Nanotechnol. Biol. Med.* **2010**, *6*, 634.
[6] N. F. Steinmetz, *Mol. Pharmaceutics* **2013**, *10*, 1.
[7] N. F. Steinmetz, V. Hong, E. D. Spoerke, P. Lu, K. Breitenkamp, M. G. Finn, M. Manchester, *J. Am. Chem. Soc.* **2009**, *131*, 17093.
[8] J. K. Pokorski, N. F. Steinmetz, *Mol. Pharmaceutics* **2011**, *8*, 29.
[9] B. C. Bundy, J. R. Swartz, *J. Biotechnol.* **2011**, *154*, 230.
[10] A. C. Steven, J. F. Conway, N. Cheng, N. R. Watts, D. M. Belnap, A. Harris, S. J. Stahl, P. T. Wingfield, *Adv. Virus Res.* **2005**, *64*, 125.
[11] A. E. Ashcroft, H. Lago, J. M. B. Macedo, W. T. Horn, N. J. Stonehouse, P. G. Stockley, *J. Nanosci. Nanotechnol.* **2005**, *5*, 2034.
[12] D. Ivanov, O. V. Tsodikov, J. Kasanov, T. Ellenberger, G. Wagner, T. Collins, *Proc. Natl. Acad. Sci. USA* **2007**, *104*, 4353.
[13] E. Blanchard, D. Brand, S. Trassard, A. Goudeau, P. Roingeard, *J. Virol.* **2002**, *76*, 4073.
[14] W. T. Horn, K. Tars, E. Grahn, C. Helgstrand, A. J. Baron, H. Lago, C. J. Adams, D. S. Peabody, S. E. V. Phillips, N. J. Stonehouse, L. Liljas, P. G. Stockley, *Structure* **2006**, *14*, 487.
[15] K. Valegard, L. Liljas, K. Fridborg, T. Unge, *Nature* **1990**, *345*, 36.
[16] R. Golmohammadi, K. Valegård, K. Fridborg, L. Liljas, *J. Mol. Biol.* **1993**, *234*, 620.
[17] R. Golmohammadi, K. Fridborg, M. Bundule, K. Valegård, L. Liljas, *Structure* **1996**, *4*, 543.
[18] M. A. Bruckman, X. Yu, N. F. Steinmetz, *Nanotechnology* **2013**, *24*, 462001.

DOI: 10.1002/smll.201601053

[19] A. Datta, J. M. Hooker, M. Botta, M. B. Francis, S. Aime, K. N. Raymond, *J. Am. Chem. Soc.* **2008**, *130*, 2546.
[20] S. Qazi, L. O. Liepold, M. J. Abedin, B. Johnson, P. Prevelige, J. A. Frank, T. Douglas, *Mol. Pharmaceutics* **2013**, *10*, 11.
[21] J. D. Lewis, G. Destito, A. Zijlstra, M. J. Gonzalez, J. P. Quigley, M. Manchester, H. Stuhlmann, *Nat. Med.* **2006**, *12*, 354.
[22] K. Li, H. G. Nguyen, X. Lu, Q. Wang, *Analyst* **2010**, *135*, 21.
[23] F. M. Brunel, J. D. Lewis, G. Destito, N. F. Steinmetz, M. Manchester, H. Stuhlmann, P. E. Dawson, *Nano Lett.* **2010**, *10*, 1093.
[24] P. L. Chariou, K. L. Lee, A. M. Wen, N. M. Gulati, P. L. Stewart, N. F. Steinmetz, *Bioconjugate Chem.* **2015**, *26*, 262.
[25] N. Stephanopoulos, G. J. Tong, S. C. Hsiao, M. B. Francis, *ACS Nano* **2010**, *4*, 6014.
[26] P. A. Suci, Z. Varpness, E. Gillitzer, T. Douglas, M. Young, *Langmuir* **2007**, *23*, 12280.
[27] J. K. Pokorski, K. Breitenkamp, L. O. Liepold, S. Qazi, M. G. Finn, *J. Am. Chem. Soc.* **2011**, *133*, 9242.
[28] S. Shukla, N. DiFranco, A. Wen, U. Commandeur, N. Steinmetz, *Cell. Mol. Bioeng.* **2015**, *8*, 433.
[29] S. Shukla, A. L. Ablack, A. M. Wen, K. L. Lee, J. D. Lewis, N. F. Steinmetz, *Mol. Pharmaceutics* **2013**, *10*, 33.
[30] N. F. Steinmetz, M. Manchester, *Biomacromolecules* **2009**, *10*, 784.
[31] K. L. Lee, S. Shukla, M. Wu, N. R. Ayat, C. E. El Sanadi, A. M. Wen, J. F. Edelbrock, J. K. Pokorski, U. Commandeur, G. R. Dubyak, N. F. Steinmetz, *Acta Biomater.* **2015**, *19*, 166.
[32] N. Ohtake, K. Niikura, T. Suzuki, K. Nagakawa, S. Mikuni, Y. Matsuo, M. Kinjo, H. Sawa, K. Ijiro, *ChemBioChem* **2010**, *11*, 959.
[33] M. Brasch, I. K. Voets, M. S. T. Koay, J. J. L. M. Cornelissen, *Faraday Discuss.* **2013**, *166*, 47.
[34] Q. Zeng, H. Wen, Q. Wen, X. Chen, Y. Wang, W. Xuan, J. Liang, S. Wan, *Biomaterials* **2013**, *34*, 4632.
[35] F. Zhao, G. Shen, C. Chen, R. Xing, Q. Zou, G. Ma, X. Yan, *Chem. – Eur. J.* **2014**, *20*, 6880.
[36] K. Liu, R. Xing, Q. Zou, G. Ma, H. Möhwald, X. Yan, *Angew. Chem. Int. Ed.* **2016**, *55*, 3036.
[37] H. Zhang, J. Fei, X. Yan, A. Wang, J. Li, *Adv. Funct. Mater.* **2015**, *25*, 1193.
[38] N.-C. Fan, F.-Y. Cheng, J.-a. A. Ho, C.-S. Yeh, *Angew. Chem. Int. Ed.* **2012**, *51*, 8806.
[39] Y. Shamay, L. Adar, G. Ashkenasy, A. David, *Biomaterials* **2011**, *32*, 1377.
[40] H.-M. Lee, D. R. Larson, D. S. Lawrence, *ACS Chem. Biol.* **2009**, *4*, 409.
[41] Z. Huang, *Technol. Cancer Res. Treat.* **2005**, *4*, 283.
[42] Z. Chen, N. Li, S. Li, M. Dharmarwardana, A. Schlimme, J. J. Gassensmith, *WIREs Nanomed. Nanobiotechnol.* **2015**, DOI: 10.1002/wnan.1379.
[43] K. S. Raja, Q. Wang, M. J. Gonzalez, M. Manchester, J. E. Johnson, M. G. Finn, *Biomacromolecules* **2003**, *4*, 472.
[44] U. Wattendorf, H. P. Merkle, *J. Pharm. Sci.* **2008**, *97*, 4655.
[45] J. V. Jokerst, T. Lobovkina, R. N. Zare, S. S. Gambhir, *Nanomedicine* **2011**, *6*, 715.
[46] E. K. Yoo, A. H. Rook, R. Elenitsas, F. P. Gasparro, B. R. Vowels, *J. Invest. Dermatol.* **1996**, *107*, 235.
[47] L. Geskin, *Skin Ther. Lett.* **2007**, *12*, 1.
[48] O. Tacar, P. Sriamornsak, C. R. Dass, *J. Pharm. Pharmacol.* **2013**, *65*, 157.
[49] M. E. B. Smith, F. F. Schumacher, C. P. Ryan, L. M. Tedaldi, D. Papaioannou, G. Waksman, S. Caddick, J. R. Baker, *J. Am. Chem. Soc.* **2010**, *132*, 1960.
[50] F. F. Schumacher, V. A. Sanchania, B. Tolner, Z. V. F. Wright, C. P. Ryan, M. E. B. Smith, J. M. Ward, S. Caddick, C. W. M. Kay, G. Aeppli, K. A. Chester, J. R. Baker, *Sci. Rep.* **2013**, *3*, 1525.
[51] F. Manzenrieder, R. Luxenhofer, M. Retzlaff, R. Jordan, M. G. Finn, *Angew. Chem. Int. Ed.* **2011**, *50*, 2601.
[52] P. G. Holder, D. T. Finley, N. Stephanopoulos, R. Walton, D. S. Clark, M. B. Francis, *Langmuir* **2010**, *26*, 17383.
[53] The purchased PEG 2000-amine has a broad weight distribution, which results in multiple bands on the SDS-PAGE after conjugation.
[54] K. Altintoprak, A. Seidenstücker, A. Welle, S. Eiben, P. Atanasova, N. Stitz, A. Plettl, J. Bill, H. Gliemann, H. Jeske, D. Rothenstein, F. Geiger, C. Wege, *Beilstein J. Nanotechnol.* **2015**, *6*, 1399.
[55] I. Ostolska, M. Wiśniewska, *Colloid Polym. Sci.* **2014**, *292*, 2453.

Received: March 28, 2016
Revised: May 16, 2016
Published online: